

Terahertz Magnon Excitations and Switching in Non-Collinear Antiferromagnets

Durga Prasad Goli^{1,*} and Se Kwon Kim^{1,†}

¹*Department of Physics, Korea Advanced Institute of Science and Technology, Daejeon 34141, Republic of Korea*
(Dated: January 3, 2025)

We investigate how spatiotemporal spin polarized current can lead to terahertz frequency excitations in non-collinear antiferromagnets. By solving the Landau-Lifshitz-Gilbert equation numerically for non-collinear antiferromagnet, we show that the magnon frequency spectrum exhibits standing spin wave modes and depends on the thickness of Mn_3Ge in heterostructure $\text{Fe}|\text{Au}|\text{Mn}_3\text{Ge}$. Also, we analyze the switching process of ground state as a function of a spin current. We show a switching phase diagram, which contains switching and non-switching regions. Our work suggests non-collinear antiferromagnets as an efficient platform for terahertz magnonics and ultrafast memory devices.

I. INTRODUCTION

The discovery of magnetization quenching [1], excitation of terahertz (THz) frequency waves [2–4], and switching [5] through femtosecond laser pulses paved the way for the emergence of femtomagnetism as a new field [6, 7]. The potential of femtosecond laser pulses to provide further insights into ultrafast magnetization dynamics has generated considerable interest. They offer new opportunities for controlling magnetization in thin magnetic layers within picoseconds. Application of a femtosecond laser pulse on a ferromagnet/nonmagnet (FM/NM) structure causes majority spin electrons to exit FM, resulting in demagnetization within a few picoseconds [8, 9]. The superdiffusion electron transport theory, introduced by Battiato et al. [10–12], explained this phenomenon. Similarly, in a spin valve comprising of two ferromagnets (FM1 and FM2) and a nonmagnetic spacer (FM1/NM/FM2), the polarized spin carriers can reach FM2 due to demagnetization in FM1 by femtosecond laser pulse [13–15]. The ultrafast polarized spin current exerts spin transfer torque (STT) on FM2, resulting the generation of THz dynamics and switching magnetization. Recent studies on ferromagnet heterostructures revealed that the excitation of magnon frequencies reportedly reached up to a few THz [13–15].

To enhance the excitation of magnon frequency range, antiferromagnets (AFM) are considered to be reliable choice over FMs. They offer several advantages, including minimal stray fields, ultrafast magnetic dynamics, and higher magnon frequencies [16, 17]. Ultrafast THz dynamics of the Néel vector in AFMs can be induced by spin currents [18] and light [19–22]. Theoretical predictions on collinear AFM revealed that ultrafast spin dynamics caused by a spin current from a femtosecond laser pulse can excite resonant magnon modes with frequencies higher than FMs [23, 24].

Going beyond conventional collinear AFMs, non-collinear antiferromagnetic (NAFM) materials like Mn_3X

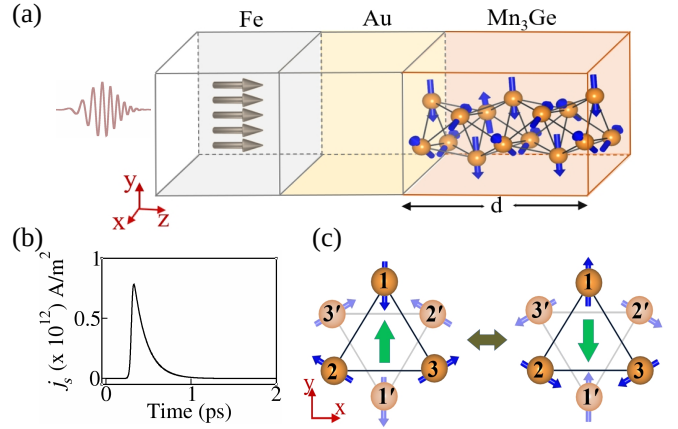


FIG. 1. (a) Schematic illustration of $\text{Fe}|\text{Au}|\text{Mn}_3\text{Ge}$ spin valve heterostructure, where a femtosecond laser pulse irradiates Fe. (b) The resultant temporal polarized spin current at Mn_3Ge using Eq. (3) with $j_0=10^{12} \text{ A/m}^2$. (c) Two degenerate ground states of Mn_3Ge , each with a magnetic unit cell of six Mn atoms within kagome bilayer and the corresponding spin texture is a 120° non-collinear ground state. Collective magnetic order of the ground state is represented by octupole moment (green arrow). It is possible to switch from one ground state to another using j_s .

($\text{X}=\text{Ir}, \text{Sn}, \text{Ge}$) are capturing interest due to their unconventional transport phenomena such as the anomalous Hall effect [25–28], anomalous Nernst effect [29, 30], and magneto-optical Kerr effect [31]. Recent studies revealed that the ultrafast dynamics [32] and deterministic switching [33] within the influence of STT in Mn_3Sn . In this paper, we demonstrate the generation of standing spin waves with high-frequency magnon modes capable of reaching several THz by considering Mn_3Ge . Taking advantage of the ultrafast Néel vector dynamics in Mn_3Ge , the switching mechanism facilitates reversal of Néel vector within a few picoseconds.

The structure of this paper is as follows. In Sec. II, we introduce a spin valve heterostructure along with the spin Hamiltonian. We describe atomistic spin simulation technique for computing the ultrafast spin dynamics due to STT on Mn_3Ge . In Sec. III, we investigate magnon spec-

* durga@kaist.ac.kr

† sekwonkim@kaist.ac.kr

trum and switching phase diagrams. We show that the emergence of standing spin waves, whose resonance frequencies can reach THz range as a function of thickness. We demonstrate that the STT induces ultrafast dynamics in the Néel vector, enabling the field-free switching in Mn₃Ge. In Sec. IV, we summarize the results.

II. MODEL AND SPIN HAMILTONIAN

We propose a heterostructure spin valve, comprising Fe|Au|Mn₃Ge as shown in Fig. 1(a). In this structure, we consider a thin film of Mn₃Ge, which is made up of AB stacked kagome lattice planes in the [0001] direction [34]. The presence of geometric frustration causes a ground state to be NAFM order with sublattice spins set at 120°. Fig. 1(c) shows that a magnetic unit cell of six Mn atoms within a kagome bilayer. The sublattice spins in layer-1 are labeled as 1, 2 and 3 whereas 1', 2' and 3' for layer-2. The corresponding spin texture is characterized by a ferroic order of cluster magnetic octupole [35, 36]. The spin Hamiltonian describing Mn₃Ge is given by

$$\begin{aligned} \mathcal{H} = & \frac{J_{\text{AFM}}^{\text{intra}}}{2} \sum_{\langle i,j \rangle} \vec{S}_i \cdot \vec{S}_j + \frac{J_{\text{FM}}^{\text{inter}}}{2} \sum_{\langle i,j' \rangle} \vec{S}_i \cdot \vec{S}_{j'} \\ & + \frac{J_{\text{AFM}}^{\text{inter}}}{2} \sum_{\langle i,j' \rangle} \vec{S}_i \cdot \vec{S}_{j'} + \frac{D^{\text{intra}}}{2} \sum_{\langle i,j \rangle} \hat{z} \cdot (\vec{S}_i \times \vec{S}_j) \\ & - K \sum_i (\vec{S}_i \cdot \hat{n}_i)^2, \end{aligned} \quad (1)$$

where the local magnetic moment of Mn at site i is defined by unit spin vector \vec{S}_i with magnitude μ_s . $\langle i, j \rangle$ and $\langle i, j' \rangle$ represent bonding between intralayer and interlayer spins. $J_{\text{AFM}}^{\text{intra}}$ is the intralayer nearest-neighbor AFM exchange interaction strength. The interlayer FM and AFM exchange strengths are represented by $J_{\text{FM}}^{\text{inter}}$ and $J_{\text{AFM}}^{\text{inter}}$ respectively. The intralayer Dzyaloshinskii-Moriya interaction is D^{intra} and K is the easy-axis in-plane anisotropy, whose sublattice vectors are $\hat{n}_1 = -\hat{y}$, $\hat{n}_2 = -(\sqrt{3}/2)\hat{x} + (1/2)\hat{y}$ and $\hat{n}_3 = (\sqrt{3}/2)\hat{x} + (1/2)\hat{y}$ (shown in Fig. 1(c)). The corresponding spin configuration is one of the degenerate ground states of Mn₃Ge. For simulations, the parameters in Eq. (1) are taken as: $J_{\text{AFM}}^{\text{intra}} = 37.4$ meV, $J_{\text{FM}}^{\text{inter}} = -18.7$ meV, $J_{\text{AFM}}^{\text{inter}} = 6.24 \times 10^{-3}$ meV, $D^{\text{intra}} = 2.18 \times 10^{-2}$ meV and $K = 10^{-3}$ meV [37, 38]. The interlayer distance between two kagome planes is taken as 2.2 Å. In this work, the size of Mn₃Ge system is taken to be $4 \times 4 \times d$ nm³, where d is thickness of Mn₃Ge. Periodic boundary conditions are implemented in the xy-plane.

The spin valve setup shown in Fig. 1(a) utilizes the superdiffusive transport theory [10, 11], implies Fe absorbs a femtosecond laser pulse, resulting in the excitation of spin electrons, polarized in the magnetization direction of Fe. To enhance the effect of STT due to polarized spin current, we assume the easy-plane of Mn₃Ge is perpendicular to the magnetization direction of Fe. Utilizing the

Landau-Lifshitz-Gilbert (LLG) equation, we carry out atomistic spin simulations on Mn₃Ge in the presence of STT. The LLG equation is integrated numerically with the support of fourth order Runge-Kutta solver. The LLG equation is expressed as follows:

$$\begin{aligned} \alpha \vec{S}_i \times \frac{\partial \vec{S}_i}{\partial t} - \frac{\partial \vec{S}_i}{\partial t} = & \gamma \vec{S}_i \times \vec{H}_i^{\text{eff}} \\ & + \frac{\gamma \hbar \theta}{2edM_s} j_s [\vec{S}_i \times (\vec{S}_i \times \hat{z})], \end{aligned} \quad (2)$$

where γ is the gyromagnetic ratio and α is the intrinsic Gilbert damping. The effective field of site i is represented by $\vec{H}_i^{\text{eff}} = -\frac{1}{\mu_s} \frac{\partial \mathcal{H}}{\partial \vec{S}_i}$. Other parameters are as follows: θ is the spin Hall angle, e is charge of an electron, d is thickness, M_s is saturation of magnetization and \hat{z} is the polarization direction of spin current. j_s is the spin current due to femtosecond laser pulse absorption of Fe. In this model, j_s is considered to be spatially dependent in Mn₃Ge as it transfers spin angular momentum to local Mn spins, impacting its magnitude [13]. Thus, the profile of j_s is presented in a spatiotemporal form as shown below:

$$j_s = j_0 e^{-z/\lambda_{\text{STT}}} \frac{e^{-t/\tau_2}}{1 + e^{-(t-t_0)/\tau_1}}. \quad (3)$$

Here j_0 is the magnitude of spin current at Au|Mn₃Ge interface, z is length of Mn₃Ge and λ_{STT} is penetration depth of spin current. The parameters t_0 , τ_1 and τ_2 characterize temporal profile of spin current. t_0 represents delay time of pulse, while τ_1 and τ_2 are exponential decay times. The values given to the parameters in Eqs. (2) and (3) are as follows: $\alpha = 0.003$, $M_s = 2.23 \times 10^5$ A/m [32] and $\mu_s = 2.5 \mu_B$. The spin Hall angle is set to be 1, adopted from Refs. [14, 39] and $\lambda_{\text{STT}} = 1$ nm to mimic experimental conditions [40]. The time step for numerical integration of Eq. (2) is 1 fs and total integration time is 500 ps. All the calculations are done at $T = 0$ K. The temporal variation of spin current is shown in Fig. 1(b) for $j_0 = 10^{12}$ A/m² and temporal parameters $t_0 = 300$ fs, $\tau_1 = 10$ fs and $\tau_2 = 150$ fs for first layer of Mn₃Ge.

III. RESULTS

First, using the atomistic spin simulation technique, we relax the spins of Mn₃Ge to the ground state as described in Eq. (1) without spin current. This can be done by integrating Eq. (2) numerically with $j_0 = 0$. After initial equilibration, we turn on j_s by taking $j_0 = 10^{12}$ A/m² to investigate the spin current effect on Mn₃Ge as a function of thickness. We set $t_0 = 300$ fs, $\tau_1 = 10$ fs and $\tau_2 = 150$ fs. STT process excites ultrafast dynamics of all Mn spins in Mn₃Ge, leading to the generation of high-frequency spin waves that propagate throughout the sample. These spin waves reflect

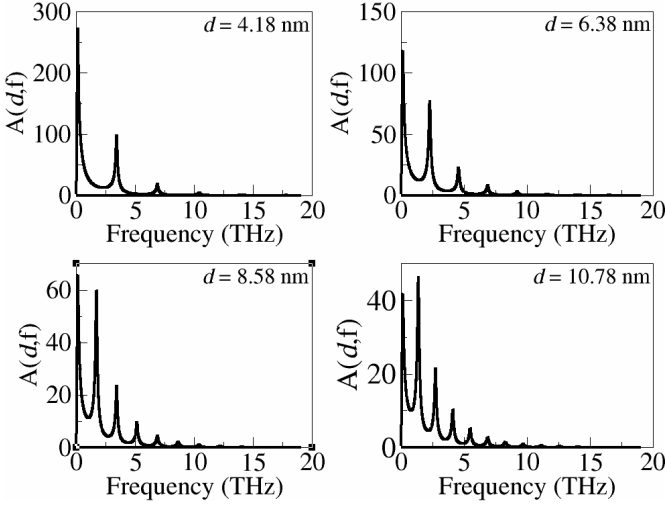


FIG. 2. Excited magnon spectrum $A(z, f)$ [Eq. (4)] at the most distant layer ($z = d$) from the spin-current source for four different thicknesses, $d = 4.18, 6.38, 8.58, 10.78$ nm. The number of magnon modes increases with the thickness.

multiple times at the open ends over hundreds of picoseconds, resulting in the formation of standing spin waves at THz frequencies. The Mn spins exhibit in-plane precession, while maintaining a non-zero z -component of the spin vector. The spin precessions include both degenerate and highly excited spin configurations. By employing the atomistic spin simulations, we examine the time evolution of z -component of each spin ($S_i^z(z, t)$) (irrespective of the sublattice and layer) for 500 ps time interval. The Fast Fourier transformations (FFT) are carried out for $S_i^z(z, t)$ to extract the frequency spectrum. The amplitudes of FFT are calculated by taking the S_i^z of each layer is given by

$$A(z, f) = \sum_{i=1}^M \sum_{j=1}^{N_{\text{steps}}} S_i^z(z, t) e^{-i2\pi ft}, \quad (4)$$

where $S_i^z(z, t)$ is z -component of i^{th} site spin as a function of thickness coordinate (z) and time t . N_{steps} is the number of integration time steps and M is number of spins per layer.

Spin excitations triggered by j_s lead to maximum spin dynamics at the resonance frequencies of Mn_3Ge , causing frequency peaks to emerge with large amplitude compared to the rest of the spectrum. To investigate the spin wave excitations, we calculate the magnon spectrum of spins in the last layer of Mn_3Ge for different thicknesses, shown in Fig. 2. Distinct peaks observed in each spectrum shows the formation of standing spin waves at resonant frequencies, regardless of film thickness. For a film of finite thickness, these standing spin waves are represented by a wave vector, $k_n = n\pi/d$ (n being an integer). The magnon spectrum span a broad range of THz frequencies and are resonantly excited with wave vectors satisfy the confinement condition of k_n . The low fre-

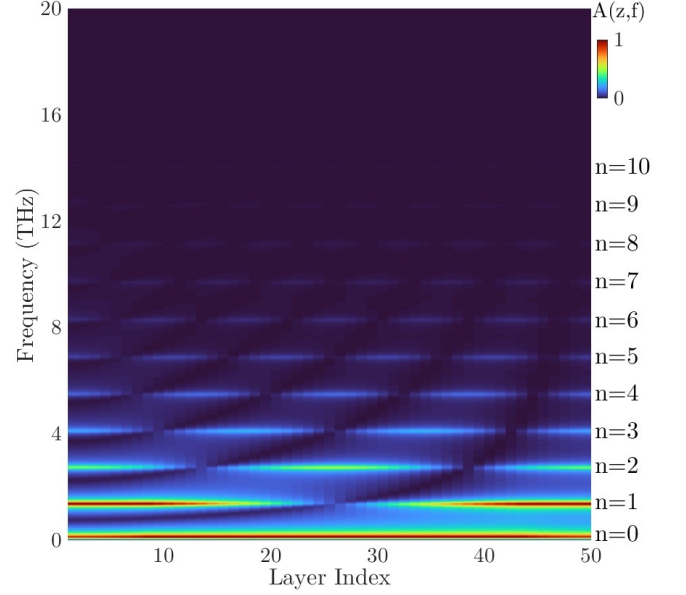


FIG. 3. Layer dependent magnon spectrum $A(z, f)$ [Eq. (4)] for the thickness, $d = 10.78$ nm with 50 layers. The number of standing spin wave modes, $n = 0, 1, 2, \dots, 10$ are appeared. Here $A(z, f)$ is the normalized FFT amplitude.

quency peak ($n = 0$) is the fundamental AFM resonance frequency of Mn_3Ge , which is 0.13 THz from Fig. 2. This peak position remains constant regardless of the thickness. As d increases, more peaks start to appear in the magnon spectrum and the separation between peaks decreases. Also, the peaks with $n > 0$ move towards lower frequencies. The amplitudes of higher frequency peaks are noticeably smaller compared to the peaks in the low frequency spectrum. This is due to fact that the spin dynamics of high frequencies being limited to a few picoseconds, while lower frequency dynamics can last for a few hundred picoseconds.

We now examine the spatial distribution of spin-wave modes in the Mn_3Ge . Fig. 3 illustrates the spatial dependent magnon spectrum for $d = 10.78$ nm with 50 layers. The FFTs are carried out for $S_i^z(z, t)$ for each layer separately over a duration of 500ps to get the layer dependent spectrum. The emergence of standing spin wave spectrum in Mn_3Ge is a result of constructive interference among the reflected spin waves. Apart from the fundamental AFM resonance mode, there are 10 visible spin wave nodes ($n = 10$) with wavelength, $\lambda = 2d/n$. The magnon spectrum does not show higher frequency modes ($n > 10$). This is due to the fact that magnon excitations of these modes have short lifetimes and are suppressed quickly by damping [13]. The standing spin wave magnon spectrum resembles the spectrum of FM and collinear AFM [14, 15, 24].

Now we present the results for switching process in Mn_3Ge . This can be identified by observing the sign change of Néel vector and change in the octupole moment

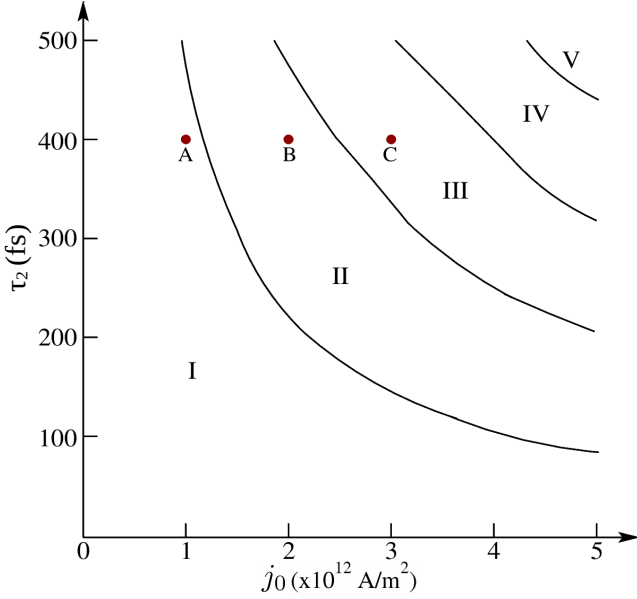


FIG. 4. Switching phase diagram as a function of j_0 and τ_2 . This plot consists of switching (II and IV) and non-switching (I, III and V) regions.

direction. For a three sublattice system, the two Néel vectors can be defined as follows: $\vec{l}_1 = (\vec{S}_1 + \vec{S}_2 - 2\vec{S}_3)/3\sqrt{2}$ and $\vec{l}_2 = (-\vec{S}_1 + \vec{S}_2)/\sqrt{6}$ [41, 42]. Below, we show our simulation results in terms of one Néel vector (\vec{l}_1) and the angle of the octupole moment with y-axis, which is denoted by ϕ_{oct} . Since it is observed that, during the spin dynamics driven by STT, the spins constituting the system preserve the 120° non-collinear configuration, we take the mirror image of \mathbf{S}_1 with respect to the xz -plane as the octupole moment [43]. As the spins rotate clockwise, the octupole moment rotates counter clockwise, fulfilling the condition of opposite handedness [44]. To observe a successful switching process, spins should gain enough energy due to j_s to overcome the anisotropy energy barrier into a new spin reversal configuration [38].

For the switching calculations, we keep $t_0 = 300$ fs and $\tau_1 = 10$ fs fixed while varying j_0 and τ_2 . Fig. 4 illustrates the switching phase diagram as a function of j_0 and τ_2 for $d = 4.18$ nm. This phase diagram consists of switching and non-switching regions. From the figure, it is evident that critical values of j_0 and τ_2 are essential for the switching process. For a better understanding, we calculate the time evolution of \vec{l}_1 and ϕ_{oct} for a few points from Fig. 4, which are labeled by A, B and C with different j_0 and $\tau_2 = 400$ fs. No switching is observed at A in region I for $j_0 = 1 \times 10^{12}$ A/m² and magnetic unit cell returns to the initial state. Only subtle dynamics observed in \vec{l}_1 and ϕ_{oct} , recovering their initial values within a few picoseconds as shown in Figs. 5(a) and (d). This is due to the temporal profile of j_s is not sufficient enough to exert STT on spins to overcome the barrier.

To realize a successful switching process, sufficiently

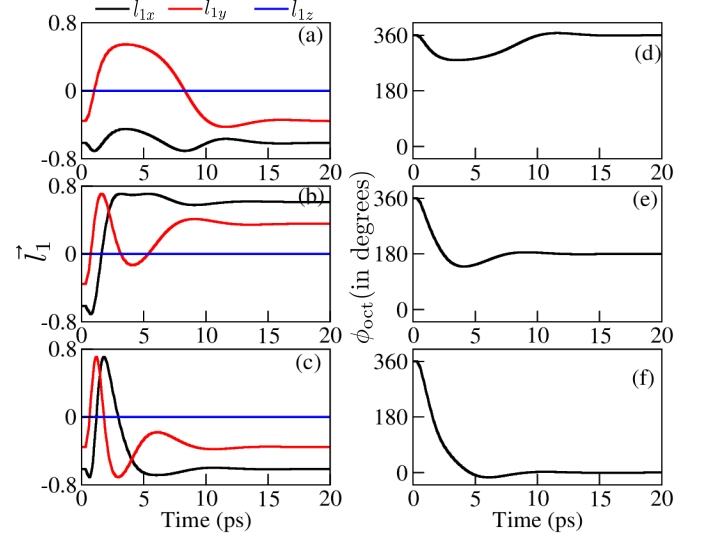


FIG. 5. The dynamics of the Néel vector, \vec{l}_1 and the angle of the magnetic octupole moment, ϕ_{oct} (with respect to the y-axis) are shown for three different j_0 values, taken from Fig. 4 indicated in red dots and are labeled as A, B and C respectively. Here $j_0 = 1 \times 10^{12}$ A/m² for (a),(d), $j_0 = 2 \times 10^{12}$ A/m² for (b),(e) and $j_0 = 3 \times 10^{12}$ A/m² for (c),(f). Successful switching is observed for $j_0 = 2 \times 10^{12}$ A/m² and is shown in (b) and (e). However, no switching process is observed in (a),(d) and (c),(f). The values of ϕ_{oct} below 0° and above 360° can be translated as $\phi_{\text{oct}} = \phi_{\text{oct}} + 360^\circ$ and $\phi_{\text{oct}} = \phi_{\text{oct}} - 360^\circ$ respectively.

large values of j_0 and τ_2 are required to overcome the barrier between the degenerate ground states. At point B in region-II, a successful switching is observed for $j_0 = 2 \times 10^{12}$ A/m², with all spins rotating 180° from the initial ground state. As shown in Figs. 5(b) and (e), sign of \vec{l}_1 is reversed and a 180° rotation of octupole moment leads to a 180° change in ϕ_{oct} . The initial and final spin configurations of a magnetic unit cell are shown in Fig. 1(c). In regions II and IV, successful switching process occurs place for all (j_0, τ_2) . In these regions, switching time depends on the magnitude of j_0 as large j_0 potentially causes shorter switching time. This illustrates one of our main results: non-collinear magnets can be switched with suitable choice of the magnitude and the pulse duration of the spin current. In region III at point C with $j_0 = 3 \times 10^{12}$ A/m², spins return to their initial state via a full 360° rotation, resulting in no switching. Figs. 5(c) and (f) show that \vec{l}_1 and ϕ_{oct} return to their initial values. The spin dynamics videos of magnetic unit cell at A, B and C are provided in Supplemental Material. Similar to region-III, spins return to their initial states in region V indicates that no switching process occurs in these regions. To ensure a successful switching process with increasing d , larger values of j_s are needed. It is also possible to observe double switching by employing two j_s pulses with a time delay of a few picoseconds between the pulses for a the combination of (j_0, τ_2) in region II

and IV. In this process, the initial spin configuration is reversed by the first pulse; a second pulse rotates all spins by another 180° , returning the system to its initial state. Recent studies revealed that the spin reversal switching other than 180° is possible in the presence external field [33, 45].

IV. DISCUSSION

The main objective of this research was theoretical investigation of THz magnon excitations in NAFM. Our study predicted that it is possible to observe THz frequency excitations in Mn_3Ge . Similar behavior was observed in Fe and Mn_2Au [14, 15, 24] and the resonant frequency spectrum spans a few THz. Despite that, our studies revealed the use of NAFMs could be advantageous for boosting the resonant frequencies higher than 10 THz. Manipulating the film thicknesses can lead to the control and excitation of resonant frequencies above the fundamental mode. We suggest that thickness can be as a tool to control resonant THz frequencies of magnetic materials.

We also showed the switching mechanism in Mn_3Ge using spin current due to femtosecond laser pulse. It is possible to control the switching process by temporal

profile of femtosecond laser pulse. An investigation was conducted on how damping affects the switching time of the Néel vector in Mn_2Au [24]. In the case of Mn_3Ge , two damping values were considered for spin dynamics [32, 38]. Therefore, it is essential to continue the investigation of switching process until experimental observations are revealed.

In conclusion, we have showed the emergence of standing spin waves through the magnon excitations in NAFM with spatiotemporal polarized spin current pulse. The magnon spectrum revealed that the excitations of THz frequency spin waves along with fundamental AFM resonance frequency. The thickness of Mn_3Ge determines how many frequency modes are present in the spin wave spectrum. Furthermore, we illustrated the switching of ground state within a few picoseconds timescale. Our work may be helpful towards THz magnonics and picosecond switching of NAFM based spintronic devices.

ACKNOWLEDGMENTS

This work was supported by Brain Pool Plus Program through the National Research Foundation of Korea funded by the Ministry of Science and ICT (NRF-2020H1D3A2A03099291).

-
- [1] E. Beaurepaire, J.-C. Merle, A. Daunois, and J.-Y. Bigot, Ultrafast spin dynamics in ferromagnetic nickel, *Phys. Rev. Lett.* **76**, 4250 (1996).
 - [2] A. Kirilyuk, A. V. Kimel, and T. Rasing, Laser-induced magnetization dynamics and reversal in ferrimagnetic alloys, *Rep. Prog. Phys.* **76**, 026501 (2013).
 - [3] T. Kampfrath, M. Battiato, P. Maldonado, G. Eilers, J. Nötzold, S. Mährlein, V. Zbarsky, F. Freimuth, Y. Mokrousov, S. Blügel, M. Wolf, I. Radu, P. M. Oppeneer, and M. Münzenberg, Terahertz spin current pulses controlled by magnetic heterostructures, *Nat. Nanotechnol.* **8**, 256 (2013).
 - [4] T. Seifert, S. Jaiswal, U. Martens, J. Hannegan, L. Braun, P. Maldonado, F. Freimuth, A. Kronenberg, J. Henrizi, I. Radu, E. Beaurepaire, Y. Mokrousov, P. M. Oppeneer, M. Jourdan, G. Jakob, D. Turchinovich, L. M. Hayden, M. Wolf, M. Münzenberg, M. Kläui, and T. Kampfrath, Efficient metallic spintronic emitters of ultrabroadband terahertz radiation, *Nat. Photonics* **10**, 483 (2016).
 - [5] C. D. Stanciu, F. Hansteen, A. V. Kimel, A. Kirilyuk, A. Tsukamoto, A. Itoh, and T. Rasing, All-optical magnetic recording with circularly polarized light, *Phys. Rev. Lett.* **99**, 047601 (2007).
 - [6] J. Walowski and M. Münzenberg, Perspective: Ultrafast magnetism and THz spintronics, *J. Appl. Phys.* **120**, 140901 (2016).
 - [7] G. Malinowski, N. Bergeard, M. Hehn, and S. Mangin, Hot-electron transport and ultrafast magnetization dynamics in magnetic multilayers and nanostructures following femtosecond laser pulse excitation, *Eur. Phys. J. B* **91**, 98 (2018).
 - [8] A. Eschenlohr, M. Battiato, P. Maldonado, N. Pontius, T. Kachel, K. Holldack, R. Mitzner, A. Föhlisch, P. M. Oppeneer, and C. Stamm, Ultrafast spin transport as key to femtosecond demagnetization, *Nat. Mater.* **12**, 332 (2013).
 - [9] N. Bergeard, M. Hehn, S. Mangin, G. Lengaigne, F. Montaigne, M. L. M. Lalieu, B. Koopmans, and G. Malinowski, Hot-electron-induced ultrafast demagnetization in Co/Pt multilayers, *Phys. Rev. Lett.* **117**, 147203 (2016).
 - [10] M. Battiato, K. Carva, and P. M. Oppeneer, Superdiffusive spin transport as a mechanism of ultrafast demagnetization, *Phys. Rev. Lett.* **105**, 027203 (2010).
 - [11] M. Battiato, K. Carva, and P. M. Oppeneer, Theory of laser-induced ultrafast superdiffusive spin transport in layered heterostructures, *Phys. Rev. B* **86**, 024404 (2012).
 - [12] P. Baláž, M. Žonda, K. Carva, P. Maldonado, and P. M. Oppeneer, Transport theory for femtosecond laser-induced spin-transfer torques, *J. Phys.: Condens. Matter* **30**, 115801 (2018).
 - [13] I. Razdolski, A. Alekhin, N. Ilin, J. P. Meyburg, V. Rodatis, D. Diesing, U. Bovensiepen, and A. Melnikov, Nanoscale interface confinement of ultrafast spin transfer torque driving non-uniform spin dynamics, *Nat. Commun.* **8**, 15007 (2017).
 - [14] H. Ulrichs and I. Razdolski, Micromagnetic view on ultrafast magnon generation by femtosecond spin current pulses, *Phys. Rev. B* **98**, 054429 (2018).
 - [15] U. Ritzmann, P. Baláž, P. Maldonado, K. Carva, and P. M. Oppeneer, High-frequency magnon excitation due

- to femtosecond spin-transfer torques, *Phys. Rev. B* **101**, 174427 (2020).
- [16] T. Jungwirth, X. Marti, P. Wadley, and J. Wunderlich, Antiferromagnetic spintronics, *Nat. Nanotechnol.* **11**, 231 (2016).
 - [17] V. Baltz, A. Manchon, M. Tsoi, T. Moriyama, T. Ono, and Y. Tserkovnyak, Antiferromagnetic spintronics, *Rev. Mod. Phys.* **90**, 015005 (2018).
 - [18] R. Cheng and Q. Niu, Dynamics of antiferromagnets driven by spin current, *Phys. Rev. B* **89**, 081105 (2014).
 - [19] A. V. Kimel, B. A. Ivanov, R. V. Pisarev, P. A. Usachev, A. Kirilyuk, and T. Rasing, Inertia-driven spin switching in antiferromagnets, *Nat. Phys.* **5**, 727 (2009).
 - [20] T. Kampfrath, A. Sell, G. Klatt, A. Pashkin, S. Mährlein, T. Dekorsy, M. Wolf, M. Fiebig, A. Leitenstorfer, and R. Huber, Coherent terahertz control of antiferromagnetic spin waves, *Nat. Photonics* **5**, 31 (2011).
 - [21] J. R. Hortensius, D. Afanasiev, M. Matthiesen, R. Leenders, R. Citro, A. V. Kimel, R. V. Mikhaylovskiy, B. A. Ivanov, and A. D. Caviglia, Coherent spin-wave transport in an antiferromagnet, *Nat. Phys.* **17**, 1001 (2021).
 - [22] J. L. Ross, P.-I. Gavriloaea, F. Freimuth, T. Adamantopoulos, Y. Mokrousov, R. F. L. Evans, R. Chantrell, R. M. Otxoa, and O. Chubykalo-Fesenko, Ultrafast antiferromagnetic switching of Mn_2Au with laser-induced optical torques, *npj Comput. Mater.* **10**, 234 (2024).
 - [23] T. Chirac, J.-Y. Chauleau, P. Thibaudau, O. Gomonay, and M. Viret, Ultrafast antiferromagnetic switching in Mn_2Au induced by spin transfer torques, *Phys. Rev. B* **102**, 134415 (2020).
 - [24] M. Weißenhofer, F. Foggetti, U. Nowak, and P. M. Oppeneer, Néel vector switching and terahertz spin-wave excitation in Mn_2Au due to femtosecond spin-transfer torques, *Phys. Rev. B* **107**, 174424 (2023).
 - [25] H. Chen, Q. Niu, and A. H. MacDonald, Anomalous Hall effect arising from noncollinear antiferromagnetism, *Phys. Rev. Lett.* **112**, 017205 (2014).
 - [26] J. Kübler and C. Felser, Non-collinear antiferromagnets and the anomalous Hall effect, *Europhys. Lett.* **108**, 67001 (2014).
 - [27] S. Nakatsuji, N. Kiyohara, and T. Higo, Large anomalous Hall effect in a non-collinear antiferromagnet at room temperature, *Nature (London)* **527**, 212 (2015).
 - [28] A. K. Nayak, J. E. Fischer, Y. Sun, B. Yan, J. Karel, A. C. Komarek, C. Shekhar, N. Kumar, W. Schnelle, J. Kübler, C. Felser, and S. S. P. Parkin, Large anomalous Hall effect driven by a nonvanishing Berry curvature in the noncollinear antiferromagnet Mn_3Ge , *Sci. Adv.* **2**, e1501870 (2016).
 - [29] M. Ikhlas, T. Tomita, T. Koretsune, M.-T. Suzuki, D. Nishio-Hamane, R. Arita, Y. Otani, and S. Nakatsuji, Large anomalous Nernst effect at room temperature in a chiral antiferromagnet, *Nat. Phys.* **13**, 1085 (2017).
 - [30] H. Reichlova, T. Janda, J. Godinho, A. Markou, D. Kriegner, R. Schlitz, J. Zelezny, Z. Soban, M. Bejarano, H. Schultheiss, P. Nemecek, T. Jungwirth, C. Felser, J. Wunderlich, and S. T. B. Goennenwein, Imaging and writing magnetic domains in the non-collinear antiferromagnet Mn_3Sn , *Nat. Commun.* **10**, 5459 (2019).
 - [31] T. Higo, H. Man, D. B. Gopman, L. Wu, T. Koretsune, O. M. J. van't Erve, Y. P. Kabanov, D. Rees, Y. Li, M.-T. Suzuki, S. Patankar, M. Ikhlas, C. L. Chien, R. Arita, R. D. Shull, J. Orenstein, and S. Nakatsuji, Large magneto-optical Kerr effect and imaging of magnetic octupole domains in an antiferromagnetic metal, *Nat. Photonics* **12**, 73 (2018).
 - [32] A. Shukla and S. Rakheja, Spin-torque-driven terahertz auto-oscillations in noncollinear coplanar antiferromagnets, *Phys. Rev. Appl.* **17**, 034037 (2022).
 - [33] H. Tsai, T. Higo, K. Kondou, T. Nomoto, A. Sakai, A. Kobayashi, T. Nakano, K. Yakushiji, R. Arita, S. Miwa, Y. Otani, and S. Nakatsuji, Electrical manipulation of a topological antiferromagnetic state, *Nature (London)* **580**, 608 (2020).
 - [34] N. Kiyohara, T. Tomita, and S. Nakatsuji, Giant anomalous Hall effect in the chiral antiferromagnet Mn_3Ge , *Phys. Rev. Appl.* **5**, 064009 (2016).
 - [35] T. Nomoto and R. Arita, Cluster multipole dynamics in noncollinear antiferromagnets, *Phys. Rev. Res.* **2**, 012045 (2020).
 - [36] S. Dasgupta, Tuning the transport properties of Mn_3Ge through the effect of strain on its magnetism, *Phys. Rev. B* **106**, 064431 (2022).
 - [37] Y. Chen, J. Gaudet, S. Dasgupta, G. G. Marcus, J. Lin, T. Chen, T. Tomita, M. Ikhlas, Y. Zhao, W. C. Chen, M. B. Stone, O. Tchernyshyov, S. Nakatsuji, and C. Broholm, Antichiral spin order, its soft modes, and their hybridization with phonons in the topological semimetal Mn_3Ge , *Phys. Rev. B* **102**, 054403 (2020).
 - [38] G. Chaudhary, A. A. Burkov, and O. G. Heinonen, Magnetism and magnetotransport in the kagome antiferromagnet Mn_3Ge , *Phys. Rev. B* **105**, 085108 (2022).
 - [39] A. Alekhin, I. Razdolski, N. Ilin, J. P. Meyburg, D. Dising, V. Roddatis, I. Rungger, M. Stamenova, S. Sanvito, U. Bovensiepen, and A. Melnikov, Femtosecond spin current pulses generated by the nonthermal spin-dependent Seebeck effect and interacting with ferromagnets in spin valves, *Phys. Rev. Lett.* **119**, 017202 (2017).
 - [40] A. Ghosh, S. Auffret, U. Ebels, and W. E. Bailey, Penetration depth of transverse spin current in ultrathin ferromagnets, *Phys. Rev. Lett.* **109**, 127202 (2012).
 - [41] O. V. Gomonay and V. M. Loktev, Using generalized Landau-Lifshitz equations to describe the dynamics of multi-sublattice antiferromagnets induced by spin-polarized current, *Low Temp. Phys.* **41**, 698 (2015).
 - [42] V. M. L. D. P. Goli and A. Manchon, Crossover from diffusive to superfluid transport in frustrated magnets, *Phys. Rev. B* **103**, 104425 (2021).
 - [43] Z. He and L. Liu, Magnetic dynamics of strained non-collinear antiferromagnet, *J. Appl. Phys.* **135**, 093902 (2024).
 - [44] J.-Y. Yoon, P. Zhang, C.-T. Chou, Y. Takeuchi, T. Uchimura, J. T. Hou, J. Han, S. Kanai, H. Ohno, S. Fukami, and L. Liu, Handedness anomaly in a non-collinear antiferromagnet under spin-orbit torque, *Nat. Mater.* **22**, 1106 (2023).
 - [45] Z. Xu, X. Zhang, Y. Qiao, G. Liang, S. Shi, and Z. Zhu, Deterministic spin-orbit torque switching including the interplay between spin polarization and kagome plane in Mn_3Sn , *Phys. Rev. B* **109**, 134433 (2024).